Electron-impact excitation of molecular nitrogen. I. Excitation of the $C\,^3\Pi_u$, $E\,^3\Sigma_g^+$, and $a''\,^1\Sigma_g^+$ states

C. P. Malone,[1,2] P. V. Johnson,[1] I. Kanik,[1] B. Ajdari,[2] and M. A. Khakoo[2]
[1]*Jet Propulsion Laboratory, California Institute of Technology, 4800 Oak Grove Drive, Pasadena, California 91109, USA*
[2]*Department of Physics, California State University, Fullerton, California 92834, USA*
(Received 19 November 2008; published 11 March 2009)

Differential cross sections (DCSs) are presented for electron-impact excitation of the $C\,^3\Pi_u$, $E\,^3\Sigma_g^+$, and $a''\,^1\Sigma_g^+$ states in N_2 from the $X\,^1\Sigma_g^+(v''=0)$ ground-state level. The DCSs were obtained from measurements of energy-loss spectra in the region of 10.75 to 12.75 eV measured at incident energies of 13, 15, 17.5, 20, 25, 30, 50, and 100 eV, and for scattering angles ranging from 5° to 130°. The results are compared with existing measurements.

DOI: 10.1103/PhysRevA.79.032704 PACS number(s): 34.80.Gs, 34.50.Bw

I. INTRODUCTION

Electron collisions with molecular nitrogen continue to garner interest due to their importance in gaseous discharge phenomena. In atmospheres with significant nitrogen compositions, such as the Earth and Titan, e^-+N_2 interactions are a necessary component of the atmospheric energy budgets. Emissions resulting from electron collisions with N_2, along with scattering of electrons via energy-loss processes, have received a significant amount of recent attention (for instance, see Refs. [1–4]). On the theoretical side, Tashiro and Morokuma [5] provided close-coupling *R*-matrix calculations for e^-+N_2 excitation of the $A\,^3\Sigma_u^+$, $B\,^3\Pi_g$, $W\,^3\Delta_u$, $B'\,^3\Sigma_u^-$, $a'\,^1\Sigma_u^-$, $a\,^1\Pi_g$, $w\,^1\Delta_u$, and $C\,^3\Pi_u$ electronic levels from the $X\,^1\Sigma_g^+(v''=0)$ ground state. Experimental electron-energy-loss measurements for excitation of these same states were addressed in terms of differential cross sections (DCSs) by Khakoo *et al.* [6] and integral cross sections (ICSs) by Johnson *et al.* [7]. Most recently, excitation of the $a''\,^1\Sigma_g^+$, $b\,^1\Pi_u$, $c_3\,^1\Pi_u$, $o_3\,^1\Pi_u$, $b'\,^1\Sigma_u^+$, $c_4'\,^1\Sigma_u^+$, $G\,^3\Pi_u$, and $F\,^3\Pi_u$ states from the $X\,^1\Sigma_g^+(v''=0)$ ground state have been investigated by our group [8–10] via electron-energy-loss measurements. Reviews of previous works are contained within these papers.

Many of the N_2 Rydberg-valence levels investigated in [8,10] predissociate. The predissociation mechanism for the $b\,^1\Pi_u$, $c_3\,^1\Pi_u$, and $o_3\,^1\Pi_u$ states of N_2 is caused indirectly by spin-orbit coupling between the $b\,^1\Pi_u$ and $C\,^3\Pi_u$ valence states, the latter of which is electrostatically coupled to the $C'\,^3\Pi_u$ valence-state continuum (e.g., see the recent coupled-channel study by Lewis *et al.* [11]). The successful unfolding of the energy-loss data by Khakoo *et al.* [8], which was complicated by the inapplicability of Franck-Condon factors (FCFs) in relation to these strongly coupled levels, provided an impetus for us to revisit the $C\,^3\Pi_u$ state, which was not fully covered previously in the work of Khakoo *et al.*[6], and where FCFs were used to account for the missing part of the $C\,^3\Pi_u$ valence state above 11.25 eV. Unlike most previous efforts (e.g., Refs. [6,12–14]), Zubek and King [15] obtained DCSs for the excitation of the $C\,^3\Pi_u$ state without utilizing FCFs in their electron-energy-loss unfolding. A similar approach is taken in the present work and the reader is referred to Paper II (Malone *et al.* [16]) for details regarding the $C\,^3\Pi_u$ state's individual vibrational-level DCSs.

The present work has also enabled an updated comparison of the $A\,^3\Sigma_u^+$, $B\,^3\Pi_g$, $W\,^3\Delta_u$, $B'\,^3\Sigma_u^-$, $a'\,^1\Sigma_u^-$, $a\,^1\Pi_g$, $w\,^1\Delta_u$, and $C\,^3\Pi_u$ state "sum" DCSs between our results and those of Trajmar *et al.* [14] and Brunger and Teubner [12], i.e., the only complete experimental investigations of all of these states. Of note, the $C\,^3\Pi_u$ and $a''\,^1\Sigma_g^+$ states were intermediates in normalizing the above-mentioned DCSs in the papers of Trajmar *et al.* [14] and Brunger and Teubner [12], respectively. The $a''\,^1\Sigma_g^+$ state DCSs were also revisited, due to the fact that this state was also covered in our experimental energy-loss range. These DCSs were used to compare with and extend our previous measurements [8,9] in terms of energy and angular coverage. Finally, we also report DCSs for the excitation of the $E\,^3\Sigma_g^+$ state from the $X\,^1\Sigma_g^+(v''=0)$ ground state, thus effectively completing our investigation of relevant neutral excited electronic states of N_2.

II. EXPERIMENT

Detailed descriptions of the experimental apparatus were given by Khakoo *et al.* [6,8]. Briefly, cylindrical electrostatic optics and double hemispherical energy selectors were utilized, both in the electron gun and in the detector. Energy-loss spectra, including both the elastic peak and the inelastic region of interest, were collected at fixed impact energies and scattering angles by repetitive multichannel-scaling techniques. The target N_2 beam was formed by effusing the gas through a thin-aperture system comprising a 0.3-mm-diameter aperture in a 0.025 mm thick brass plate (see Khakoo *et al.* [17] for details) with the target gas driven through it with a backing pressure of about 2 Torr. This replaced the capillary array arrangement that was used in our previous N_2 studies [6,8,9]. The present gas-source setup was used previously in the measurement of elastic DCSs [18] and corroborates our previous results as shown in the present paper. The incident energy E_0 of the electron beam was calibrated using the procedures discussed by Khakoo *et al.* [8]. The correct value of E_0 could be readily set to within ± 50 meV by adjusting the appropriate electron-gun bias power supply. The spectrometer was found to be very stable, yielding currents of about 7–20 nA with an energy resolution of approximately 40–65 meV full width at half maximum (FWHM).

The procedure for obtaining normalized cross sections consisted of several steps. The spectrometer was tuned in an iterative manner for each E_0 at the scattering angle (θ) of 90°, with the background-gas signal removed using the movable source method developed by Hughes *et al.* [19]. This was performed so that the elastic-to-inelastic ratios closely reproduced those from the time-of-flight (TOF) work of LeClair and Trajmar [20] (at θ=90°), which are accurate on a relative scale to ±15%. The analyzer was baked and maintained in a very clean vacuum environment so that this response remained stable.

Additional transmission checks and corrections to the energy-loss spectra were made at the lowest residual energies ($E_R=E_0-E$, where E is the energy loss). Individual excitation functions (scattered intensity at a fixed angle as a function of impact energy) for the $X\,^1\Sigma_g^+(v''=0)\rightarrow C\,^3\Pi_u$ ($v'=0,1,2$), $E\,^3\Sigma_g^+(v'=0)$, and $a''\,^1\Sigma_g^+(v'=0)$ levels were measured at selected fixed angles between 15° and 130° and then calibrated against He as follows. First, for E_0 from 10 to 20 eV, background-corrected (using our movable source setup [19]) elastic He-electron scattering was measured as a function of E_0 at a fixed θ of 90°. This gave (as E_R remained above 10 eV) a measurement of the source strength at the collision region after being checked against well-established elastic-scattering DCSs [21]. This was confirmed from the fact that this correction did not vary from the calibration DCS curve by more than approximately 10%. Second, we measured background-corrected He electron-impact energy-loss spectra at E_0=30 eV and θ=90°, covering the ionization continuum, from which the spectrometer's transmission function with respect to E_R could be determined using methods detailed in Refs. [22,23]. The product of the source-strength correction (mainly electron-gun dependent) and transmission correction (mainly analyzer dependent) was used to calibrate the excitation functions at all θ. However, when applying this check, it was observed that at our smallest θ, DCSs of the $E\,^3\Sigma_g^+(v'=0,1)$ and $a''\,^1\Sigma_g^+(v'=0,1)$ states, taken at the lowest E_0 of 13 eV (therefore also lowest E_R) needed to be recorrected for normalization to elastic scattering. This was done by further measuring excitation functions (i.e., fixed angle with varying E_0) for these states and adjusting the transmission based on these excitation functions (see later). This additional adjustment was needed probably because of systematic errors incurred in the analysis of the data [e.g., background counts in this region of the energy-loss spectrum and the precision in reproducing signal rates at forward scattering θ values (i.e., $\theta<30°$) in our experiment, compounded by the steep rise from threshold] in determining inelastic-to-elastic ratios at these small angles from our prior DCS determinations. However, at larger scattering angles the present DCS measurements (at fixed E_0 and varying θ) and the independently observed excitation functions (at fixed θ and varying E_0) were in very good agreement.

Energy-loss spectra were accumulated in the energy-loss range of 10.75–12.75 eV and consequently unfolded, leaving all vibrational levels of the $C\,^3\Pi_u(v'=0-4)$ state as independent features, rather than using FCFs to fix their relative intensities. For the $E\,^3\Sigma_g^+(v'=0,1,2)$ and $a''\,^1\Sigma_g^+(v'=0,1)$ states, the $v'=0$ features overwhelmingly dominate the remaining levels (for instance, see details in Refs. [8,9]). As such, fitting higher vibronic levels independently would carry increased uncertainty. Therefore, only the $v'=0$ levels of the $E\,^3\Sigma_g^+$ and $a''\,^1\Sigma_g^+$ states were fitted (independently), with the FCFs of Table I used to account for the remaining v'-level contributions (i.e., scaling to the fitted $v'=0$ intensities). Transition energies for the features in the energy-loss region of interest were taken from Table I of Khakoo *et al.* [6] and Table I of Khakoo *et al.* [8], and, for the $X\,^1\Sigma_g^+(v''=0)\rightarrow E\,^3\Sigma_g^+(v'=0,1)$ transitions, were obtained using the spectroscopic tables of Lofthus and Krupenie [24]. Using the Rydberg-Klein-Rees (RKR) code of Gilmore *et al.* [25,26] and the spectroscopic data of Lofthus and Krupenie

TABLE I. Summary of energy-loss (E) values and FCFs for the excitation of the spectral features of N_2 used in the present work. Note that the $C\,^3\Pi_u$ state v' levels were not FCF-fitted in the spectrum, but rather as independent v' features. However, their FCFs from RKR calculations (see text) are given here (italicized) for reference only.

Summary of N_2 excited states used			
E (eV)	State	v'	FCF
10.902	$a'\,^1\Sigma_u^-$	15	0.0223
10.919	$B'\,^3\Sigma_u^-$	17	0.0135
10.969	$a\,^1\Pi_g$	13	0.0014
10.989	$w\,^1\Delta_u$	12	0.0424
11.032	$C\,^3\Pi_u$	0	*0.5468*
11.048	$a'\,^1\Sigma_u^-$	16	0.0163
11.056	$B'\,^3\Sigma_u^-$	18	0.0097
11.131	$a\,^1\Pi_g$	14	0.0007
11.146	$w\,^1\Delta_u$	13	0.0314
11.190	$a'\,^1\Sigma_u^-$	17	0.0115
11.279	$C\,^3\Pi_u$	1	*0.3074*
11.290	$a\,^1\Pi_g$	15	0.0004
11.300	$w\,^1\Delta_u$	14	0.0228
11.330	$a'\,^1\Sigma_u$	18	0.0081
11.452	$w\,^1\Delta_u$	15	0.0163
11.467	$a'\,^1\Sigma_u^-$	19	0.0056
11.520	$C\,^3\Pi_u$	2	*0.1059*
11.601	$w\,^1\Delta_u$	16	0.0115
11.748	$w\,^1\Delta_u$	17	0.0081
11.752	$C\,^3\Pi_u$	3	*0.0296*
11.877	$E\,^3\Sigma_g^+$	0	0.903
11.891	$w\,^1\Delta_u$	18	0.0056
11.973	$C\,^3\Pi_u$	4	*0.0074*
12.139	$E\,^3\Sigma_g^+$	1	0.093
12.253	$a''\,^1\Sigma_g^+$	0	0.850
12.416	$E\,^3\Sigma_g^+$	2	0.004
12.500	$b\,^1\Pi_u$	0	0.010
12.516	$a''\,^1\Sigma_g^+$	1	0.150
12.575	$b\,^1\Pi_u$	1	0.057
12.663	$b\,^1\Pi_u$	2	0.126
12.750	$b\,^1\Pi_u$	3	0.230

[24], we obtained FCFs for the $X\,^1\Sigma_g^+(v''=0)\rightarrow E\,^3\Sigma_g^+(v'=0,1)$ transitions. These results are summarized in Table I. We note that any variation in the FCFs for $E\,^3\Sigma_g^+(v'>0)$ between the present FCF results and other data sets (primarily Refs. [24–26]) had an insignificant influence on our unfolded results due to the overwhelming contribution of the $v'=0$ levels.

Regions clear of energy-loss features determined the background of the inelastic energy-loss spectra. The line shape used for fitting each vibronic transition in the energy-loss region was determined empirically by nonlinear least-squares fitting of a multi-Gaussian function to the isolated $a''\,^1\Sigma_g^+(v'=0)$ feature, which was found to be consistent with other well-resolved features. Hence, the energy-loss region of interest was fitted in each multichannel spectrum by means of a nonlinear least-squares algorithm to all features in the present work, similar to that employed by Khakoo *et al.* [8] (with the exception noted above). The overall fitting yielded a relative DCS, which was normalized to an absolute DCS standard (as discussed later). Two further adjustments resulted in further improving the fits to the spectrum: the beginning of the energy-loss range and the step size δE (i.e., energy-loss increment per channel) for the nonlinear least-squares fit to the experimental spectra could be varied to further minimize the chi-squared goodness of the fit.

Our total spectral intensities were placed on an absolute DCS scale by comparing well-established absolute elastic DCSs (see discussion below) with our simultaneously measured spectra covering the elastic and inelastic energy-loss regions. Spectra were measured using the movable-source method [18,19] with the gas source aligned with the electron beam (signal+background; in), and then moved out of alignment (background; out). This was executed for all E_0 with an angular coverage between 5° and 130° in various angular increments. The subtracted results of the out spectra from the in spectra were used to determine the ratios of relative inelastic DCSs of the summed $C+E+a''$ states, including some vibronic contributions from other overlapping states as determined from Table I of Khakoo *et al.* [6,8] (see our Table I), to the relative elastic DCSs. This procedure accurately accounted for background signals (particularly for elastic spectra) using the movable-source method and eliminated possible geometrical scattering issues (i.e., angular-dependent scattering volume) via the simultaneously measured inelastic-to-elastic ratios. These experimental efforts were performed consecutively for each E_0 to minimize possible system variations, though we found the experiment to be very stable over the course of the work.

The summed $C+E+a''$ DCS data were renormalized using the inelastic-to-elastic DCS ratios of LeClair and Trajmar [20], their "region II" at $\theta=90°$, which have an uncertainty of less than ≈5%. We note that the minimization of transmission effects (discussed above) improved the quality of the data by requiring relatively small transmission corrections via Ref. [20] to the inelastic energy-loss results. Inelastic-scattering contributions from other (weaker) overlapping states were taken into account by including these levels in the overall fit. A summary of these additional features used in the unfolding of our energy-loss spectra is also given in Table I. This procedure correctly removed contributions of the $B'\,^3\Sigma_u^-(v'=17,18)$, $a'\,^1\Sigma_u^-(v'=15-19)$, $a\,^1\Pi_g(v'=13-15)$, and $w\,^1\Delta_u(v'=12-18)$ levels, which were not of interest in this work. Spectral data for these features were based on the values in Table I of Khakoo *et al.* [6,8]. At $\theta=90°$, the fractional contributions of these weak features to the unfolded, independently fitted $C\,^3\Pi_u(v'=0,1,2,3,4)$, $E\,^1\Sigma_g^+(v'=0)$, and $a''\,^1\Sigma_g^+(v'=0)$ levels were approximately 0, 0.072, 0.056, 0.059, 0.052, 0.048, 0.047, and 0.018, respectively. Table I shows that the $E\,^3\Sigma_g^+(v'=1)$ level at $E=12.139$ eV did not overlap with the $a''\,^1\Sigma_g^+(v'=0)$ level at $E=12.253$ eV. We also note from Table I that the FCFs for the $E\,^3\Sigma_g^+(v'=0,1,2)$ levels leave only an unaccounted FCF of less than 0.4% for all $v'>1$.

The normalized inelastic-to-elastic ratios are listed in Table II. Inelastic-to-elastic ratios were then obtained for each unfolded inelastic feature by comparing the individual relative intensities of the vibrational features of each electronic state with the summed intensities. This procedure minimizes uncertainties in our analysis involving the spectrometer transmission and results in more accurate relative inelastic DCSs over extended energy-loss ranges. Note that the inelastic-to-elastic ratio ordinarily covered the complete inelastic E range from 10.75 to 12.75 eV. However, at small θ and low E_R, there are systematic problems in applying this to the full inelastic E range at our lowest E_0. The $E_0=13$ eV inelastic-to-elastic ratios were therefore recalibrated using excitation functions as discussed earlier. A full investigation of such excitation functions, for the $C\,^3\Pi_u(v'=0,1,2)$, $E\,^3\Sigma_g^+(v'=0)$, and $a''\,^1\Sigma_g^+(v'=0)$ states, is described in a forthcoming paper.

Absolute inelastic DCSs for the $X\,^1\Sigma_g^+(v''=0)\rightarrow C\,^3\Pi_u(v'=0-4)$, $E\,^3\Sigma_g^+(v'=0-2)$, and $a''\,^1\Sigma_g^+(v'=0,1)$ transitions were then obtained by multiplying the inelastic-to-elastic ratios to an average of selected experimental DCSs for elastic electron scattering from N_2 of Srivastava *et al.* [27] (corrected in [14]), Shyn and Carignan [28] (corrected in [14]), Nickel *et al.* [29], and Gote and Ehrhardt [30]. These data were tabulated by Trajmar *et al.* [14] and Brunger and Buckman [31]. In our selection, we used those values of elastic-scattering DCSs that agreed within their combined quoted uncertainties. Consequently, absolute inelastic DCSs for each unfolded feature were obtained with the effective absolute inelastic DCSs for each electronic state within the inelastic region of interest. Although we have recently measured absolute elastic DCSs [18], which agreed with previous DCSs within uncertainties, we have chosen to use the previous set of elastic DCSs applied by Khakoo *et al.* [6,8,9] to minimize any systematic uncertainty in the normalization method (i.e., our present measurement is on "equal elastic footing" with our previous measurements as far as elastic-scattering normalizations are concerned).

Overall, the experimental uncertainty assigned to each quantity is the quadrature sum of the contributing uncertainty components. For the DCS values associated with the sum of the three state excitations at 90°, we considered the statistical and fitting uncertainties in the individual scattering intensities (typically 2%–25%), the inelastic-to-elastic ratio uncertainty of the TOF results of LeClair and Trajmar [20] (≈10%), the uncertainties in the available elastic-scattering DCSs (≈14%), the uncertainty propagated by the present

TABLE II. Inelastic-to-elastic ratios R for electron scattering from N_2, determined using the movable-source method [18,19]. The inelastic ratio spans the energy-loss window of 10.75–12.75 eV where vibrational levels of electronic states, other than $C\,^3\Pi_u$, $E\,^3\Sigma_g^+$, and $a''\,^1\Sigma_g^+$, have been removed as discussed in the text. Also provided are the average percentage uncertainties over all covered angles and at each E_0.

Angle (deg)	Inelastic-to-elastic ratios R							
	13 eV	15 eV	17.5 eV	20 eV	25 eV	30 eV	50 eV	100 eV
5				0.00941		0.0186	0.00751	0.0113
10	0.00343	0.00721		0.00939	0.00886	0.0160	0.00620	0.00399
15	0.00442	0.00807	0.00634	0.00905	0.00667	0.0116	0.00546	0.00204
17		0.00850		0.00910				
20	0.00512	0.00867	0.00667	0.00906	0.00534	0.00858	0.00622	0.00258
22		0.00838		0.00910				
24		0.00839		0.00896				
25	0.00593		0.00665		0.00497	0.00827	0.00670	
26		0.00862		0.00913				
28		0.00891		0.00946				
30	0.00634	0.00888	0.00723	0.00998	0.00553	0.00867	0.00766	0.00778
32		0.00928		0.0102				
35	0.00714	0.00978	0.00844	0.0112	0.00673	0.0101	0.00988	
40	0.00787	0.0102	0.0101	0.0136	0.00832	0.0122	0.0122	0.0113
45	0.00823	0.0118	0.0127	0.0163	0.0109	0.0163	0.0156	
50	0.00879	0.0135	0.0152	0.0201	0.0145	0.0202	0.0202	0.0124
60	0.0108	0.0204	0.0241	0.0322	0.0252	0.0347	0.0273	0.0132
65	0.0146	0.0270	0.0334	0.0414	0.0351	0.0457	0.0303	
70	0.0169	0.0353	0.0443	0.0520	0.0412	0.0564	0.0366	0.0121
80	0.0258	0.0568	0.0723	0.0862	0.0610	0.0769	0.0525	0.0113
85	0.0329	0.0689	0.0805	0.0979	0.0663	0.0797	0.0578	
90	0.0374	0.0735	0.0805	0.0932	0.0675	0.0828	0.0601	0.0104
100	0.0300	0.0555	0.0600	0.0681	0.0607	0.0733	0.0528	0.00989
105	0.0239	0.0460	0.0476	0.0579	0.0520	0.0642	0.0403	
110	0.0208	0.0400	0.0401	0.0503	0.0461	0.0572	0.0331	0.00969
120	0.0154	0.0326	0.0303	0.0397	0.0361	0.0422	0.0247	0.00970
125	0.0137	0.0308	0.0288	0.0369	0.0324	0.0372	0.0217	
130	0.0135	0.0307	0.0275	0.0332	0.0292	0.0324	0.0211	0.0107
Average error	8%	5%	5%	4%	5%	4%	6%	3%

inelastic-to-elastic ratio measurements ($\approx 5\%$), and an additional uncertainty of $\approx 10\%$ for the transmission function. This resulted in a total quadrature-sum uncertainty of typically between 15% and 25% and up to approximately 37% in the worst case (see Table III).

III. RESULTS AND DISCUSSION

Table III [(a)–(h)] enumerates the DCSs and associated uncertainties for the electron-impact excitation of the transitions measured in this work. These DCSs are compared with existing measurements in Figs. 1, 3, and 4. Figure 2 compares the "sum" DCSs from several groups for the $A\,^3\Sigma_u^+$, $B\,^3\Pi_g$, $W\,^3\Delta_u$, $B'\,^3\Sigma_u^-$, $a'\,^1\Sigma_u^-$, $a\,^1\Pi_g$, $w\,^1\Delta_u$, and $C\,^3\Pi_u$ states. The inelastic DCSs of Trajmar *et al.* [14] were a renormalization of the data of Cartwright *et al.* [13,32] and included extrapolated data not found in the original work. Here, the DCSs of Trajmar *et al.* [14] have been displayed at a reduced angular range, without their extrapolated data, in order to provide a consistent coverage of experimental data throughout this paper, including data taken from the figures of Cartwright *et al.* [13]. Of note, the $E_0=17$ eV data of Trajmar *et al.* [14] are compared with the 17.5 eV data of the present work and other data sets. We now address the DCSs for the individual excitations.

A. Excitation of the $C\,^3\Pi_u$ state

Figure 1 shows the DCSs for excitation of the $C\,^3\Pi_u$ state in the energy-loss interval of this work, i.e., summed over the measured $v'=0-4$ levels, at E_0 values of 13, 15, 17.5, 20, 25, 30, 50, and 100 eV. Details of the individual $C\,^3\Pi_u(v')$

TABLE III. DCSs for the electron-impact excitation of the $X\ ^1\Sigma_g^+(v''=0) \rightarrow C\ ^3\Pi_u$, $E\ ^3\Sigma_g^+$, and $a''\ ^1\Sigma_g^+$ transitions in N_2. The inelastic DCSs are given in units of 10^{-18} cm^2 sr^{-1}. Also provided are the average percentage uncertainties over all covered angles and at each E_0.

		$C\ ^3\Pi_u$		$E\ ^3\Sigma_g^+$		$a''\ ^1\Sigma_g^+$	
	Angle (deg)	DCS	Error	DCS	Error	DCS	Error
(a) $E_0=13$ eV	10	8.88	1.65	0.479	0.121	6.37	1.24
	15	10.4	1.9	0.515	0.128	5.66	1.13
	20	11.1	2.0	0.503	0.130	5.04	0.97
	25	11.4	2.1	0.562	0.139	3.49	0.68
	30	11.2	2.1	0.599	0.145	2.46	0.47
	35	11.6	2.1	0.595	0.143	1.87	0.36
	40	11.5	2.1	0.605	0.142	1.10	0.21
	45	10.9	2.0	0.572	0.140	0.923	0.179
	50	10.3	1.9	0.572	0.152	0.730	0.144
	60	9.48	1.74	0.529	0.142	0.366	0.073
	65	10.2	1.9	0.395	0.121	0.237	0.049
	70	8.75	1.60	0.371	0.113	0.0977	0.0217
	80	7.71	1.42	0.317	0.093	0.132	0.028
	85	9.08	1.66	0.281	0.079	0.126	0.027
	90	11.6	2.1	0.251	0.070	0.219	0.047
	100	11.8	2.2	0.222	0.061	0.306	0.063
	105	10.2	1.9	0.221	0.061	0.506	0.100
	110	9.67	1.77	0.189	0.059	0.498	0.098
	120	8.78	1.61	0.160	0.050	0.397	0.079
	125	8.51	1.57	0.144	0.043	0.370	0.075
	130	8.91	1.63	0.136	0.040	0.472	0.093
	Average error		18%		27%		20%
(b) $E_0=15$ eV	10	20.1	3.0	0.672	0.148	15.6	2.6
	15	20.6	3.1	0.811	0.176	13.3	2.2
	17	21.5	3.2	0.653	0.150	12.3	2.0
	20	22.0	3.3	0.915	0.198	9.85	1.62
	22	19.5	2.9	0.797	0.170	8.92	1.43
	24	18.8	2.8	0.849	0.178	8.00	1.29
	26	19.5	2.9	0.889	0.181	6.75	1.09
	28	19.4	2.9	0.838	0.180	6.00	0.96
	30	19.0	2.9	0.745	0.175	5.43	0.88
	32	19.5	2.9	0.664	0.158	4.98	0.80
	35	19.3	2.9	0.634	0.172	3.71	0.60
	40	17.3	2.6	0.570	0.154	2.88	0.47
	45	17.4	2.6	0.575	0.149	1.83	0.30
	50	16.4	2.5	0.504	0.124	1.58	0.26
	60	17.1	2.6	0.366	0.090	1.33	0.22
	65	18.5	2.8	0.231	0.057	1.31	0.22
	70	19.9	3.0	0.169	0.043	0.943	0.157
	80	21.9	3.3	0.111	0.033	1.01	0.17
	85	23.2	3.5	0.126	0.038	1.02	0.17
	90	22.3	3.3	0.115	0.033	0.983	0.167
	100	18.2	2.7	0.101	0.028	0.939	0.157
	105	16.5	2.5	0.115	0.030	0.929	0.156
	110	16.9	2.5	0.124	0.033	0.988	0.166

TABLE III. (*Continued.*)

		$C\,^3\Pi_u$		$E\,^3\Sigma_g^+$		$a''\,^1\Sigma_g^+$	
	Angle (deg)	DCS	Error	DCS	Error	DCS	Error
	120	18.4	2.8	0.140	0.037	1.05	0.18
	125	20.2	3.0	0.161	0.042	1.03	0.17
	130	23.4	3.5	0.185	0.049	1.14	0.19
	Average error		15%		25%		17%
(c)E_0=17.5 eV	15	10.2	1.6	1.09	0.18	9.60	1.56
	20	9.61	1.46	0.744	0.122	7.24	1.21
	25	11.0	1.7	0.841	0.148	4.64	0.74
	30	10.6	1.6	0.608	0.100	3.22	0.53
	35	10.8	1.7	0.488	0.078	2.86	0.45
	40	11.7	1.8	0.344	0.054	2.67	0.43
	45	12.6	1.9	0.376	0.057	2.60	0.42
	50	11.6	1.8	0.341	0.056	2.37	0.38
	60	13.1	2.0	0.155	0.029	1.73	0.28
	65	14.3	2.2	0.198	0.038	1.60	0.26
	70	15.4	2.4	0.108	0.025	1.50	0.24
	80	17.0	2.6	0.0906	0.0205	1.27	0.20
	85	16.0	2.5	0.183	0.039	1.41	0.23
	90	14.5	2.2	0.212	0.042	1.37	0.22
	100	12.6	1.9	0.325	0.063	1.43	0.23
	105	11.6	1.8	0.350	0.066	1.34	0.22
	110	11.2	1.7	0.271	0.051	1.38	0.22
	120	11.4	1.8	0.242	0.055	1.48	0.24
	125	12.1	1.9	0.294	0.067	1.57	0.25
	130	13.8	2.1	0.221	0.047	1.67	0.27
	Average error		15%		20%		16%
(d) E_0=20 eV	5	5.51	0.84	2.62	0.69	24.3	4.0
	10	6.83	1.04	2.60	0.69	18.1	2.9
	15	8.03	1.22	2.57	0.73	11.5	1.9
	17	8.69	1.32	2.49	0.66	9.49	1.55
	20	9.92	1.52	2.13	0.55	7.17	1.17
	22	9.78	1.49	1.78	0.46	5.33	0.87
	24	9.95	1.52	1.76	0.43	4.25	0.69
	26	9.85	1.51	1.36	0.36	3.62	0.59
	28	10.2	1.6	1.25	0.38	3.10	0.52
	30	10.6	1.6	1.17	0.36	3.23	0.54
	32	10.2	1.6	0.894	0.328	3.43	0.56
	35	9.83	1.51	0.753	0.275	3.33	0.54
	40	9.79	1.51	0.653	0.225	3.74	0.61
	45	9.79	1.49	0.357	0.115	3.20	0.52
	50	9.64	1.48	0.333	0.105	2.87	0.47
	60	10.6	1.6	0.320	0.097	2.00	0.33
	65	11.1	1.7	0.280	0.086	1.73	0.28
	70	11.6	1.8	0.261	0.096	1.57	0.26
	80	13.2	2.0	0.352	0.129	1.69	0.28
	85	12.6	1.9	0.439	0.151	1.60	0.26

TABLE III. (*Continued.*)

		$C\,^3\Pi_u$		$E\,^3\Sigma_g^+$		$a''\,^1\Sigma_g^+$	
	Angle (deg)	DCS	Error	DCS	Error	DCS	Error
	90	11.5	1.8	0.461	0.149	1.39	0.22
	100	10.4	1.6	0.632	0.199	1.80	0.29
	105	10.8	1.7	0.595	0.187	1.96	0.32
	110	10.7	1.6	0.611	0.192	2.17	0.35
	120	11.1	1.7	0.406	0.128	2.54	0.42
	125	11.5	1.8	0.352	0.111	2.86	0.47
	130	11.3	1.7	0.239	0.075	2.73	0.44
	Average error		15%		31%		16%
(e) E_0=25 eV	10	2.40	0.36	3.49	0.95	29.3	4.8
	15	2.32	0.35	3.02	0.82	10.1	1.7
	20	1.89	0.29	1.86	0.54	3.27	0.52
	25	2.33	0.35	1.27	0.35	2.30	0.38
	30	3.10	0.48	1.18	0.32	3.96	0.63
	35	3.46	0.53	0.873	0.229	4.96	0.80
	40	3.98	0.61	0.871	0.219	4.09	0.65
	45	4.20	0.64	0.758	0.207	3.89	0.62
	50	4.63	0.71	1.11	0.35	3.39	0.55
	60	4.92	0.76	1.33	0.42	2.78	0.44
	65	6.35	0.98	1.28	0.49	2.41	0.39
	70	5.93	0.91	0.997	0.376	1.95	0.31
	80	6.57	1.01	0.877	0.312	2.06	0.33
	85	6.09	0.93	0.775	0.258	2.11	0.34
	90	5.99	0.92	0.774	0.251	2.29	0.37
	100	6.77	1.04	0.721	0.225	2.72	0.44
	105	7.57	1.17	0.605	0.191	3.19	0.51
	110	7.27	1.12	0.585	0.222	3.68	0.59
	120	8.47	1.30	0.486	0.184	5.38	0.86
	125	9.23	1.43	0.567	0.202	5.90	0.96
	130	9.26	1.42	0.474	0.158	5.91	0.95
	Average error		15%		32%		16%
(f) E_0=30 eV	5	3.21	0.49	4.28	0.98	64.1	10.4
	10	3.04	0.46	2.51	0.61	20.9	3.5
	15	2.81	0.43	2.45	0.70	7.85	1.25
	20	2.82	0.43	1.56	0.42	2.73	0.45
	25	3.55	0.54	1.25	0.32	3.57	0.57
	30	3.82	0.58	0.837	0.214	4.48	0.72
	35	2.89	0.44	0.626	0.153	3.54	0.57
	40	3.68	0.56	0.730	0.194	3.63	0.58
	45	4.04	0.62	0.854	0.258	3.13	0.50
	50	3.69	0.57	0.794	0.243	2.54	0.41
	60	5.40	0.83	0.913	0.335	2.22	0.35
	65	5.07	0.78	0.611	0.223	1.85	0.30
	70	5.50	0.85	0.558	0.192	1.65	0.27
	80	5.61	0.86	0.424	0.137	1.48	0.24
	85	5.41	0.83	0.353	0.111	1.35	0.22

TABLE III. (*Continued.*)

		$C\,^3\Pi_u$		$E\,^3\Sigma_g^+$		$a''\,^1\Sigma_g^+$	
	Angle (deg)	DCS	Error	DCS	Error	DCS	Error
	90	5.31	0.82	0.366	0.111	1.40	0.23
	100	5.67	0.87	0.315	0.097	1.66	0.26
	105	5.91	0.91	0.274	0.101	1.72	0.27
	110	5.90	0.91	0.238	0.087	1.96	0.31
	120	6.44	0.99	0.224	0.077	2.70	0.44
	125	6.56	1.00	0.213	0.069	3.20	0.51
	130	6.89	1.06	0.281	0.088	3.91	0.63
	Average error		15%		31%		16%
(g) E_0=50 eV	5	1.40	0.21	2.68	1.04	68.4	11.4
	10	2.63	0.40	2.05	0.56	16.9	2.9
	15	2.13	0.33	0.942	0.305	5.55	0.91
	20	1.75	0.27	0.384	0.116	0.836	0.141
	25	2.29	0.35	0.123	0.044	2.13	0.35
	30	2.01	0.31	0.0893	0.0246	2.63	0.43
	35	1.67	0.26	0.176	0.061	3.35	0.55
	40	1.74	0.27	0.128	0.039	2.72	0.44
	45	1.45	0.22	0.185	0.064	2.67	0.44
	50	1.79	0.28	0.158	0.055	2.27	0.37
	60	1.70	0.26	0.0829	0.0353	1.57	0.26
	65	1.78	0.28	0.0476	0.0202	1.31	0.21
	70	1.41	0.22	0.0717	0.0286	1.28	0.21
	80	2.07	0.32	0.0383	0.0142	0.928	0.152
	85	2.04	0.31	0.0427	0.0155	0.895	0.149
	90	2.18	0.34	0.0498	0.0173	0.742	0.123
	100	2.39	0.37	0.0415	0.0146	0.555	0.091
	105	2.44	0.38	0.0251	0.0107	0.532	0.087
	110	2.18	0.34	0.0348	0.0147	0.723	0.118
	120	2.24	0.35	0.0718	0.0286	1.68	0.28
	125	2.44	0.38	0.0957	0.0356	2.08	0.34
	130	2.45	0.38	0.217	0.079	2.54	0.42
	Average error		16%		37%		17%
(h) E_0=100 eV	5	0.259	0.039	0.737	0.142	42.4	7.1
	10	0.490	0.075	0.255	0.070	9.17	1.60
	15	0.869	0.133	0.0592	0.0192	1.82	0.30
	20	1.20	0.18	0.0303	0.0091	2.31	0.39
	30	1.18	0.18	0.0432	0.0127	3.84	0.62
	40	0.826	0.127	0.0404	0.0117	1.86	0.31
	50	0.516	0.080	0.0200	0.0055	1.04	0.17
	60	0.407	0.063	0.0196	0.0059	0.807	0.131
	70	0.297	0.046	0.0178	0.0062	0.612	0.101
	80	0.230	0.036	0.0241	0.0085	0.587	0.096
	90	0.192	0.030	0.0173	0.0074	0.573	0.094
	100	0.171	0.026	0.0184	0.0078	0.619	0.101
	110	0.161	0.025	0.0107	0.0043	0.663	0.111
	120	0.170	0.026	0.0130	0.0048	0.788	0.129

TABLE III. (*Continued.*)

Angle (deg)	$C\,^3\Pi_u$		$E\,^3\Sigma_g^+$		$a''\,^1\Sigma_g^+$	
	DCS	Error	DCS	Error	DCS	Error
130	0.287	0.044	0.0184	0.0067	1.06	0.18
Average error		16%		34%		17%

state DCSs, for $v'=0$, 1, 2, 3, and 4, are discussed in Paper II (Malone *et al.* [16]). Comparison of the present values with the DCSs of Khakoo *et al.* [6] indicates that the present $C\,^3\Pi_u$ state DCSs have been revised upward for electron-impact energies of up to approximately 20 eV. The present DCSs at $E_0=15$ eV have a pronounced change in shape at smaller angles. These differences occur in an energy range where non-Franck-Condon behavior can be expected. Intermediate energies of about $E_0=30-50$ eV are mostly unchanged within the experimental uncertainties. The $E_0=100$ eV DCSs suggest a slight decrease in the present data relative to that of Khakoo *et al.* [6].

The present $C\,^3\Pi_u$ state DCSs, and that from Khakoo *et al.* [6], are compared with available data in Fig. 1. At $E_0=13$ eV, the present DCSs are compared with the FCF-unfolded results of Khakoo *et al.* [6] at $E_0=12.5$ eV. It is not clear whether the significant increase in DCSs as a function of E_0 is due to the use of FCFs in the unfolding of Ref. [6], the rapid increase in the $C\,^3\Pi_u$ state excitation function (for instance, see Poparic *et al.* [33]), or a combination of the two. However, the results of Zobel *et al.* (see LeClair and Trajmar [20]) definitely indicate a steep rise from threshold via the increasing $C\,^3\Pi_u$ state DCSs (for $v'=0-2$) at electron-impact energies of 11.6, 12, 12.5, and 13 eV as shown in Fig. 1 (13 eV panel) from bottom to top (labeled D to A, respectively). The DCS of Zobel *et al.* (see LeClair and Trajmar [20]) at $E_0=13$ eV shows excellent agreement with the present DCS at 90°. The DCSs of Tashiro and Morokuma [5] at $E_0=12.5$ eV is shown in Fig. 1 (13 eV panel), which corresponds roughly with the 12 eV DCS of Zobel *et al.* (see LeClair and Trajmar [20]). Of note, core excited resonances were listed by Mazeau *et al.* [34] at 12.54 eV ($^2\Pi_u$) and 13.00 eV ($^2\Sigma_u^-$) for the $C\,^3\Pi_u(v'=0)$ state, which could result in intensity variations between data sets due to energy calibration uncertainties (e.g., E_0 and resolution).

At $E_0=15$ eV, the uniform transmission result of LeClair and Trajmar [20], for the essentially full $C\,^3\Pi_u(v'=0-3)$ state, is consistent with the present result at 90° (as expected) and varies slightly from that of Khakoo *et al.* [6] probably (systematically) due to the use of FCFs in their unfolding method and to account for unmeasured $C\,^3\Pi_u(v'=2-4)$ electronic-vibronic spectrum as well as small possible variations in their instrument response function. We note that only the inelastic-to-elastic ratios for the "region I" of LeClair and Trajmar [20] were used in the earlier work in Ref. [6]. This did not include the $C\,^3\Pi_u$ state in the overall normalization analysis and may have led to some inconsistent treatment for the $C\,^3\Pi_u$ state in our previous work [6], which could have been avoided if the whole $C\,^3\Pi_u$ state had been covered. Here, our analysis includes the full $C\,^3\Pi_u$ state and relies primarily on normalization to the $\theta=90°$ "region II" DCS of LeClair and Trajmar [20], which directly covers the energy-loss region of interest. The close-coupled *R*-matrix results of Tashiro and Morokuma [5] are in better shape agreement with the present DCSs, which also have approximately the same magnitude. The measured DCSs of Trajmar *et al.* [14] and Brunger and Teubner [12] are noticeably larger; however, their DCSs would be in better agreement with ours (within experimental uncertainty estimations) if the results of LeClair and co-workers [20,35] had been available to similarly account for inelastic-to-elastic transmission corrections.

Similar to the present work, Zubek and King [15] did not employ FCFs in unfolding their energy-loss data at $E_0=17.5$ and 20 eV. Their $C\,^3\Pi_u$ state DCSs agree excellently with the present DCSs. Additional discussion of the results of Zubek and King [15], along with those of Zobel *et al.* (see Ref. [20]) and LeClair and Trajmar [20], can be found in Paper II (Ref. [16]). The $E_0=17.5$ eV results of Tashiro and Morokuma [5] are larger in intensity but show reasonable shape agreement with the present results around $\theta=20°-80°$. (See Ref. [5] for further discussion of the $C\,^3\Pi_u$ state calculation issues.) The DCSs of Trajmar *et al.* [14] are in excellent agreement with both those of Zubek and King [15] and the present data, with some divergence between the data sets above approximately 90°. The magnitude of the DCSs of Brunger and Teubner [12] at $E_0=17.5$ and 20 eV is generally not in agreement with the other measurements, including the present results. Furthermore, their shape is also in disagreement with the other data sets. Again, the $E_0=20$ eV (actually 20.7 eV) DCS of LeClair and Trajmar [20] is in very good agreement with the present data, where the slight difference is attributable to the partial vibrational coverage ($v'=0-2$) and the slightly different elastic DCSs used in normalizing the respective data sets in Ref. [20].

At $E_0=30$ and 50 eV, we observe (Fig. 1) good agreement in both shape and magnitude of the DCSs of Brunger and Teubner [12] and the present data. The differing shapes of the Brunger and Teubner data [12] at $E_0=17.5$ and 20 eV, relative to the other measured data sets, cannot be easily explained considering that agreement with their DCSs is observed with other results at larger incident energies. (It is possible that the use of FCFs, instead of individual vibronic levels, in unfolding their data may have contributed to the observed deviations at lower E_0 values.) Near 70° at $E_0=30$ eV and near 50° at $E_0=50$ eV, the DCSs of Trajmar *et al.* [14] also deviate from the other data sets, but otherwise have good agreement at other covered angles. The early DCSs of Fliflet *et al.* [36], obtained from distorted-wave calculations, are generally in poor absolute agreement for all of

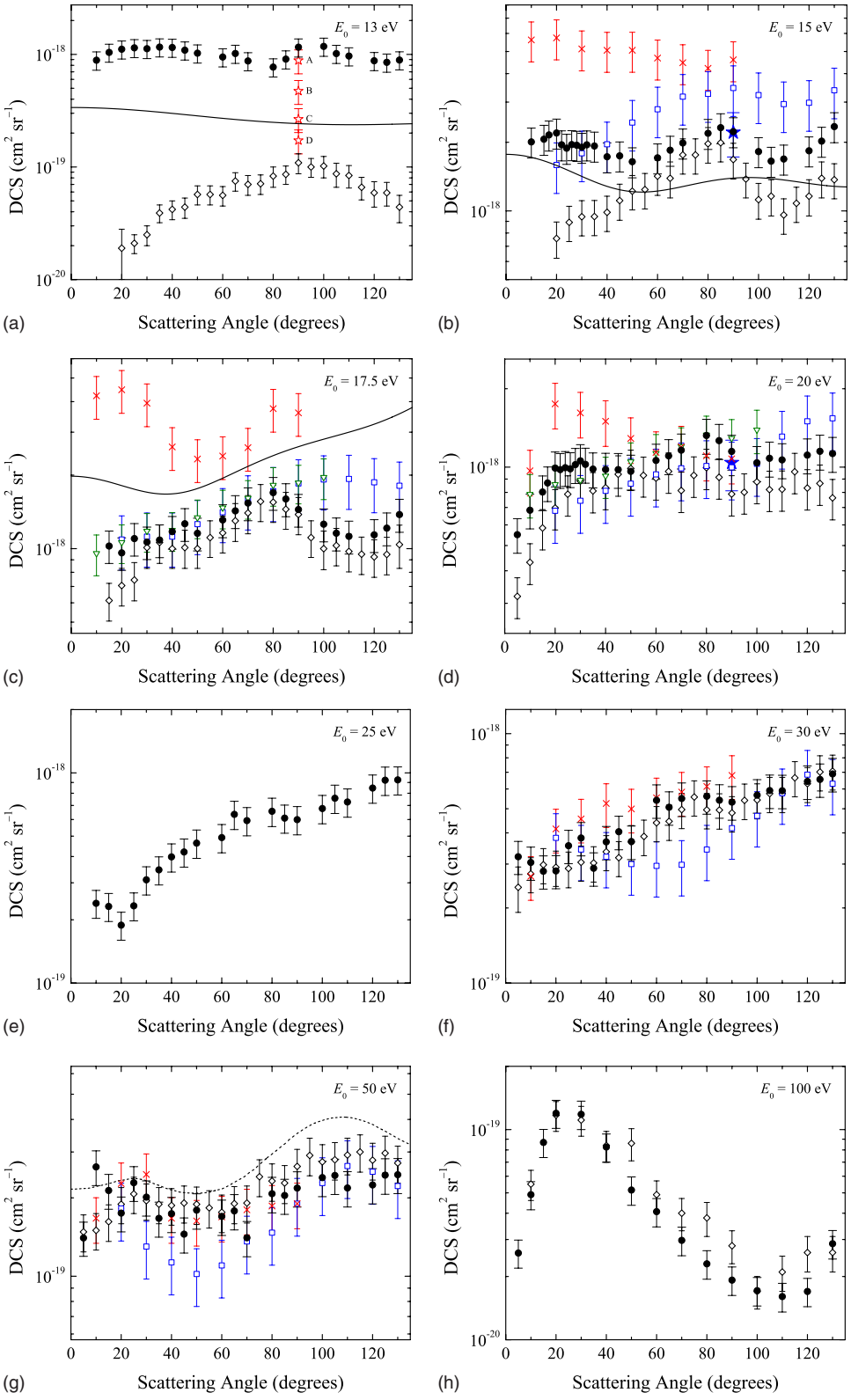

FIG. 1. (Color online) DCSs for the electron-impact excitations to the $C\,^3\Pi_u$ state with E_0 indicated on the figure panels. The E_0 =13 eV panel includes the data of Zobel *et al.* (see LeClair and Trajmar [20]) labeled as A–D, which are, respectively, 13, 12.5, 12, and 11.6 eV. Legend: ●, present work; ◇, Khakoo *et al.* [6]; □, Trajmar *et al.* [14] (17.5 eV actually at E_0=17 eV; estimated DCSs masked); ×, Brunger and Teubner [12]; ▽, Zubek and King [15]; ★, LeClair and Trajmar [20] (20 eV actually at E_0=20.7 eV with v'=0–2); ☆, Zobel *et al.* (see LeClair and Trajmar [20]); —, Tashiro and Morokuma [5]; ----, Fliflet *et al.* [36]. DCS units are in cm^2 sr^{-1}. See text for further details.

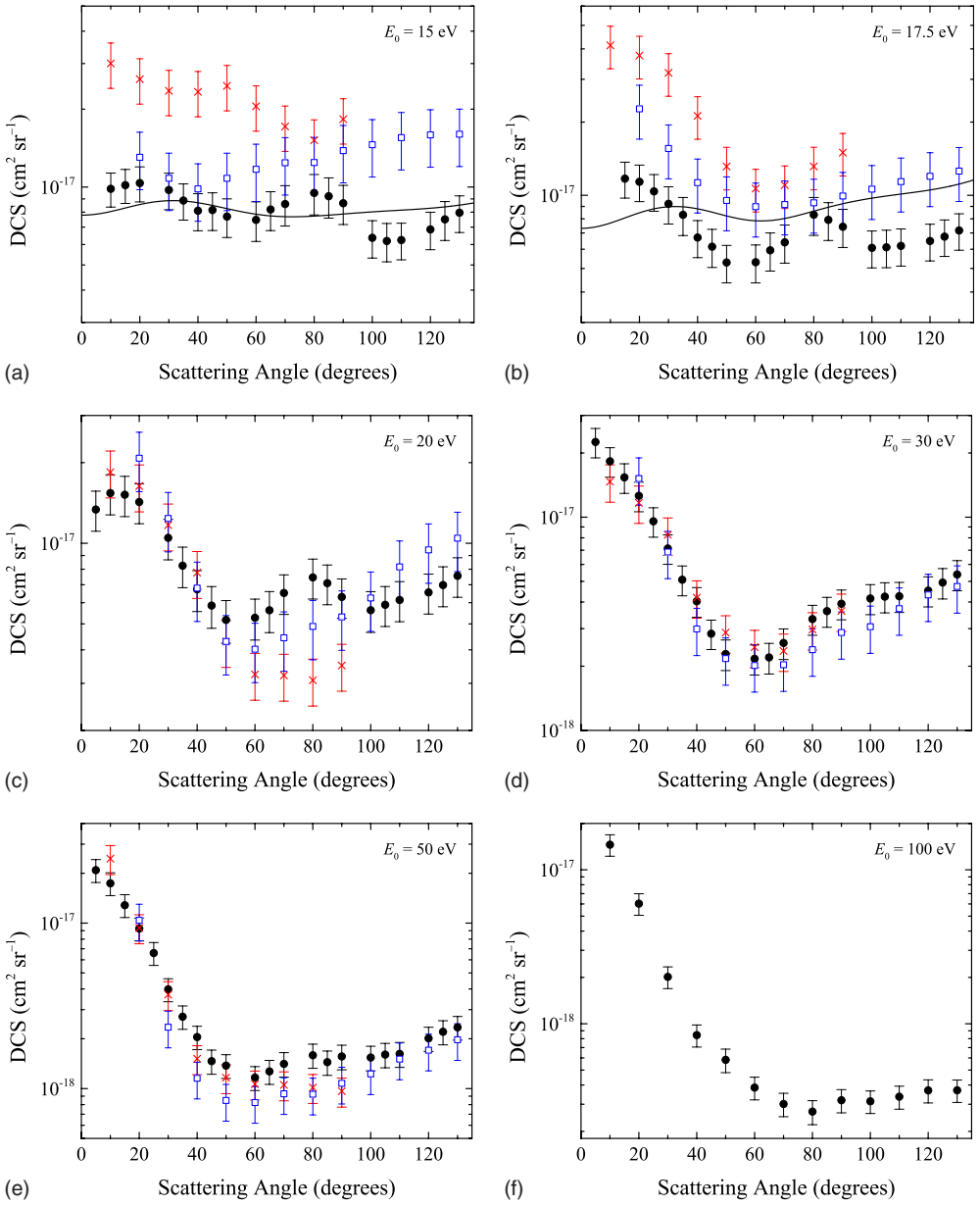

FIG. 2. (Color online) DCSs for the electron-impact excitations to the sum of the $A\ ^3\Sigma_u^+ + B\ ^3\Pi_g + W\ ^3\Delta_u + B'\ ^3\Sigma_u^- + a'\ ^1\Sigma_u^- + a\ ^1\Pi_g + w\ ^1\Delta_u + C\ ^3\Pi_u$ states with E_0 indicated on the figure panels. Legend: ●, present results combined with those of Khakoo *et al.* [6] (see text); □, Trajmar *et al.* [14] (17.5 eV actually at E_0=17 eV); ×, Brunger and Teubner [12]; —, Tashiro and Morokuma [5]. DCS units are in cm^2 sr^{-1}.

the covered electronic states. This is not unexpected as these are essentially intermediate-energy, selected coupling calculations and would not account for the many interstate close couplings in this region of the N_2 spectrum at low energies. These calculations are therefore not generally included in the current plots. However, we note that at E_0=50 eV their $C\ ^3\Pi_u$ state DCSs show good agreement in both magnitude and shape with the present data as shown in Fig. 1.

Summed DCSs revisited

Replacing the earlier $C\ ^3\Pi_u$ state DCSs of Khakoo *et al.* [6] with the presently obtained $C\ ^3\Pi_u$ state DCSs enables an updated comparison of the summed DCSs for the $A\ ^3\Sigma_u^+$, $B\ ^3\Pi_g$, $W\ ^3\Delta_u$, $B'\ ^3\Sigma_u^-$, $a'\ ^1\Sigma_u^-$, $a\ ^1\Pi_g$, $w\ ^1\Delta_u$, and $C\ ^3\Pi_u$ states between the results of our group and those of Trajmar *et al.* [14] and Brunger and Teubner [12]. Figure 2 shows sum DCSs at E_0 values common to the present work and that of Khakoo *et al.* [6]: 15, 17.5, 20, 30, 50, and 100 eV. Though a significant change in DCS magnitude was observed near threshold for the present $C\ ^3\Pi_u$ state relative to Khakoo *et al.* [6], the large DCS rate of change as a function of electron-impact energy precluded revisiting the sum DCS near E_0 =12.5–13 eV.

The changes to the sum DCSs, via the revisions of the present work, were small, but significant, being dominated by the relatively large sum intensity of other states compared

to the intensity of the individual $C\ ^3\Pi_u$ state. The revised sum DCSs generally agree with the sum values of Khakoo *et al.* [6] within uncertainties. Most noticeable were changes to the sum DCS values at $E_0=15$ eV for small angles.

Figure 2 indicates very good agreement between the present data and the sum DCSs of Trajmar *et al.* [14] and Brunger and Teubner [12] at larger electron-impact energies. The 30 and 50 eV data sets are almost entirely in agreement, while the 20 eV data sets have a slight deviation near 80°, but otherwise agree (within uncertainties) almost entirely throughout the range of overlapping measured angular values. This suggests that overall the same energy-loss spectra were measured by different groups, but differences in unfolding the multitude of vibrational features of the electronic states has resulted in differences to the individual DCSs and consequently to the derived ICSs. However, of note, the present data versus that of Brunger and Teubner [12] (with Trajmar *et al.* [14] falling approximately in between) suggest that the difference between the sum DCSs at $E_0=20$ eV in the angular region around 80° results from differences in the DCSs of the $A\ ^3\Sigma_u^+$, $B\ ^3\Pi_g$, $W\ ^3\Delta_u$, and $B'\ ^3\Sigma_u^-$ states (see Fig. 7 of Ref. [6]) on the low E region of the energy-loss range.

Clear divergence is evident at smaller electron-impact energies (15 and 17.5 eV) when comparing the results of Trajmar *et al.* [14] and Brunger and Teubner [12] with the present work. A factor of roughly 2–3 is apparent between the largest and smallest values, although the overall broad DCS shapes appear similar. Also available for comparison are the summed close-coupled R-matrix results of Tashiro and Morokuma [5], which did not previously exist in discussion by Khakoo *et al.* [6]. The summed DCSs of Tashiro and Morokuma [5] are not in full agreement (within *experimental* uncertainties) with any one measured data set, but indicate a general consistency with the present data, particularly at $E_0=15$ eV.

B. Excitation of the $E\ ^3\Sigma_g^+$ state

Figure 3 shows the DCSs for excitation of the $E\ ^3\Sigma_g^+$ state in the energy-loss interval of this work for numerous incident energies (see above). At $E_0=13$ eV, the present work indicates a broad maximum in the DCSs at approximately 40°, which is not symmetric about 90° (as was assumed by Poparic *et al.* [37] while comparing the nonabsolute data of Mazeau *et al.* [34]). We are not aware of other presently available absolute DCSs at 13 eV to compare with. Again, we note that Mazeau *et al.* [34] listed core excited (Feshbach) resonances in this case near 13 eV ($^2\Sigma_u^-$) for the $E\ ^3\Sigma_g^+(v'=0,1)$ state. At $E_0=15$ eV, the present DCSs indicate a maximum near 25° and exhibit an emerging minimum near 90°, which also appears in the DCSs (at different E_0) of Mazeau *et al.* [34] and Poparic *et al.* [37,38]. The DCSs of Trajmar *et al.* [14] and Brunger and Teubner [12] are somewhat inconsistent with the present results, though the reduced angular ranges contribute to uncertainty in their overall DCS shapes.

The present DCSs at $E_0=17.5$ eV have an apparent minimum near 75° and show reasonable agreement in shape (including the minimum) with that of Zubek and King [15], which is larger by a factor of ~1.7 over the entire angular range. Those of Brunger and Teubner [12] agree with the present DCSs at larger scattering angles (including the apparent minimum near 75°), but tend quantitatively toward the DCSs of Zubek and King [15] for roughly $\theta<50°$, and consequently exhibit shape disagreement outside of error bars. The DCSs of Trajmar *et al.* [14] are overall in reasonable quantitative agreement, but do not show good shape agreement.

At $E_0=20$ eV, the DCSs of Zubek and King [15] agree excellently with the present work, both with minima near 65°. Those of Brunger and Teubner [12] also exhibit a minimum near 65°, but again deviate from the present results at roughly $\theta<50°$. Those of Trajmar *et al.* [14] are in good agreement with the present $E\ ^3\Sigma_g^+$ state DCSs, but their shape eventually diverges at roughly $\theta>80°$. The present results demonstrate a consistently evolving structure with the $E_0=25$ eV DCSs having a local minimum that appears near 40°.

Figure 3 shows the present DCSs at $E_0=30$ eV, which exhibits a minimum at about 35°. Also displayed are the DCSs of Brunger and Teubner [12] that agree very well with the present results (within uncertainties), including the apparent minimum. DCSs of Trajmar *et al.* [14] deviate from the other data sets at approximately $\theta>35°$ and seem to follow an exponential decay. At $E_0=50$ eV, the present data decrease quickly through small scattering angles, show a minimum near 90° and a narrower minimum at about 30°, and suggest a backscatter component to the DCSs. The agreement between data of Trajmar *et al.* [14] and the present data is very good for measured values. Data of Brunger and Teubner [12] also have very good agreement over measured values, except at about 30°, where a local maximum is shown corresponding to the present minimum. The present DCSs at $E_0=100$ eV are small.

C. Excitation of the $a''\ ^1\Sigma_g^+$ state

Figure 4 shows DCSs for excitation of the $a''\ ^1\Sigma_g^+$ state at incident electron energies ranging from 13 to 100 eV. We have included this additional measurement on the DCSs for the $X\ ^1\Sigma_g^+(v''=0)\rightarrow a''\ ^1\Sigma_g^+(v'=0,1)$ excitation in order to verify the "dip" structure near 20°. Much of the discussion of this DCS structure is in papers of Khakoo *et al.* [8,9]. This "extra" measurement served as a check of our earlier investigations of this energy-loss range bordering the $C\ ^3\Pi_u$ and $E\ ^3\Sigma_g^+$ states. Further, the $a''\ ^1\Sigma_g^+(v'=0)$ line provides an unobstructed feature for obtaining the line shape used in the unfolding process (see above discussion and Ref. [8]). Consequently, a comparison of the presently determined $a''\ ^1\Sigma_g^+$ state DCSs with previous measurements, including that from our own group using a different gas collimating source (see above discussion), is included here. Further, we have extended our previous results to include $E_0=13$ and 15 eV and extended our angular coverage at $E_0=100$ eV.

The DCSs at $E_0=13$ eV seem to have a minimum near 75° and increase in magnitude toward small angles. We are not aware of other measurements to compare with at 13 eV. Once again, we note that core excited resonances were listed

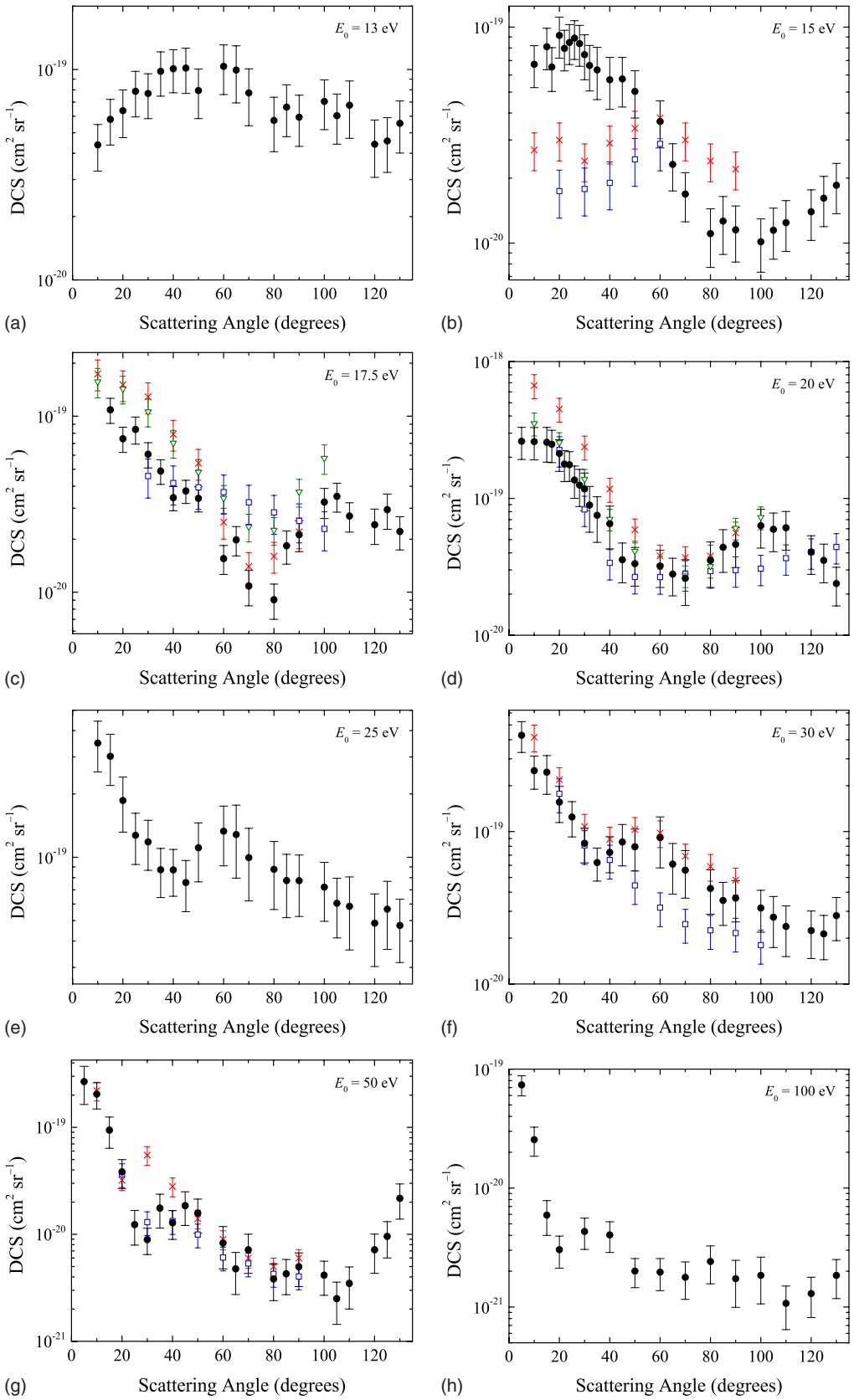

FIG. 3. (Color online) DCSs for the electron-impact excitations to the $E\,^3\Sigma_g^+$ state with E_0 indicated on the figure panels. Legend: ●, present work; □, Trajmar *et al.* [14] (17.5 eV actually at E_0=17 eV; estimated DCSs masked); ×, Brunger and Teubner [12]; ▽, Zubek and King [15]. DCS units are in cm^2 sr^{-1}.

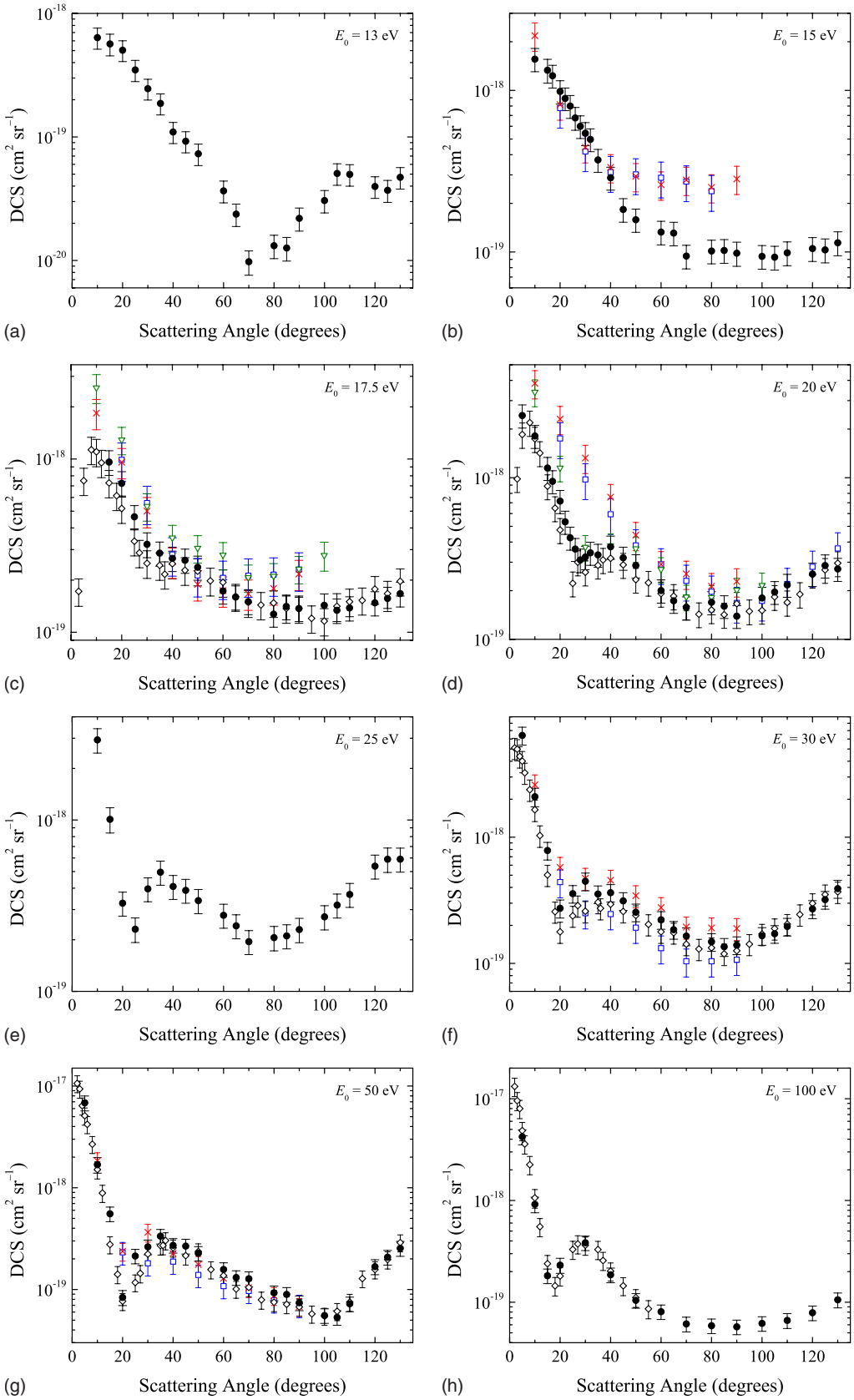

FIG. 4. (Color online) DCSs for the electron-impact excitations to the $a''\ ^1\Sigma_g^+$ state with E_0 indicated on the figure panels. Legend: ●, present work; ◇, Khakoo *et al.* [8] (scaled by 1.3 only for E_0=17.5 eV; see text); □, Trajmar *et al.* [14] (17.5 eV actually at E_0=17 eV; estimated DCSs masked); ×, Brunger and Teubner [12]; ▽, Zubek and King [15]. DCS units are in cm^2 sr^{-1}.

by Mazeau *et al.* [34] in this case near 13 eV ($^2\Sigma_u^-$) for the $a''\ ^1\Sigma_g^+(v'=0)$ state. At $E_0=15$ eV, the present results are compared with the DCSs of Trajmar *et al.* [14] and Brunger and Teubner [12]. The present DCSs have a similar shape peaking toward smaller angles (such as the 13 eV data) along with approximately the same intensity, but DCSs of Trajmar *et al.* [14] and Brunger and Teubner [12] show a decrease in DCS magnitude that levels off higher than the present results at larger scattering angles. After rechecking our results and not being able to uncover a reason for this divergence near 40°, we are reasonably confident of our DCSs. The reason for this deviation is not obvious; however, we note that our data demonstrate a trend that appears consistent as a function of incident electron energies. Slight changes in E_0 values could be contributing to the differences in data sets since the DCSs change rather quickly from threshold.

At $E_0=17.5$ eV, Fig. 4 indicates a consistent shape between the present work and that from Khakoo *et al.* [8,9]. One main difference between the 17.5 eV panel of Fig. 4 and Fig. 3(a) of Khakoo *et al.* [8] is that the 17.5 eV data from Ref. [8] have been scaled to match our present $a''\ ^1\Sigma_g^+$ state DCS at 90°. Thus the $a''\ ^1\Sigma_g^+$ state DCS values in Table III(a) of Khakoo *et al.* [8] should be adjusted upward by a factor of 1.295. After revisiting our earlier work, we remain unsure of the underlying reason for this scaling adjustment; however, the other data sets of Ref. [8] for other incident energies are consistent with the present work in both shape and intensity, within experimental uncertainties, with no justifiable impetus for scaling. It is possible that a systematic error in the spectrometer transmission calibration occurred while applying the "region II" transmission results of LeClair and Trajmar [20] for the $a''\ ^1\Sigma_g^+$ state data set at $E_0=17.5$ eV in Ref. [8], noting that all other electronic states measured by Khakoo *et al.* [8] resided in "region III" of Ref. [20].

The present DCSs at $E_0=17.5$ eV indicate good agreement with the DCSs of Trajmar *et al.* [14] and Brunger and Teubner [12] in the angular range of about 40°–70°, while those of Zubek and King [15] have a comparable shape but are globally larger in magnitude. Divergence is observed for smaller and larger angles even with the dip feature emerging in our data sets. It is probable that transmission-function differences between different groups induced the global shift in DCSs. Local shape differences are probably due to overall statistical variations, or may be due to the determination of background signal in the experiments.

Figure 4 shows our DCSs at $E_0=20$ eV along with the data of the same groups that were shown at 17.5 eV. Our present results are systematically (slightly) larger than our previous data [8], but not outside of the experimental uncertainties. Results of Zubek and King [15] demonstrate excellent structure agreement with the present results, even hinting at the dip feature near 20° via their "shoulder" at about 30°, which Trajmar *et al.* [14] and Brunger and Teubner [12] did not resolve. However, despite disagreement by a factor of ~1.5, the DCS shapes at angles >70° show improved agreement with the earlier work relative to the 17.5 eV results. The present data illustrate a consistently evolving shape that transitions from 20 to 25 eV and onward to 30 eV.

Our $E_0=30$ eV DCSs agree very well within experimental uncertainties with our previous data. Besides confirming the dip feature and the degree of backscatter, our DCSs are in between the DCSs of Trajmar *et al.* [14] and Brunger and Teubner [12] with overall good agreement (besides the dip region) within stated uncertainties. At $E_0=50$ eV, Fig. 4 again indicates good agreement with all shown data sets, disregarding the dip feature, which we have presently resolved. The backscatter in the 50 eV data is also shown to be the same as our previous measurements. Our $E_0=100$ eV DCSs still show the dip feature along with some degree of backscatter.

IV. CONCLUSIONS

We have obtained improved DCSs for electron-impact excitation of the $C\ ^3\Pi_u$, $E\ ^3\Sigma_g^+$, and $a''\ ^1\Sigma_g^+$ states in N_2 from the $X\ ^1\Sigma_g^+(v''=0)$ ground-state level. The DCSs for excitation of the investigated states were obtained by unfolding the energy-loss spectra without using FCFs in order to account for observed non-Franck-Condon behavior for the $C\ ^3\Pi_u$ state excitation. Additional details of the vibrationally resolved excitation of the $C\ ^3\Pi_u$ state are discussed in Paper II (Malone *et al.* [16]). Further, we have revisited the $a''\ ^1\Sigma_g^+$ state using an updated gas collimating system due to our recent observations of a dip feature in the DCSs [8,9]. This has allowed us to verify our previously observed structure and DCS intensities and to extend the range of measurement in energy and angle. It also drew attention to an apparent experimental error, which suggests that the 17.5 eV $a''\ ^1\Sigma_g^+$ state DCSs of Khakoo *et al.* [8] may need to be adjusted upward (approximately by a factor of 1.3). While studying this energy-loss region, we have completed the coverage of valence states in N_2 by obtaining measurements of the $E\ ^3\Sigma_g^+$ state.

ACKNOWLEDGMENTS

This work was performed at the California State University, Fullerton and at the Jet Propulsion Laboratory, California Institute of Technology, under a contract with the National Aeronautics and Space Administration (NASA). We gratefully acknowledge financial support through the National Science Foundation, under Grant No. NSF-PHY-RUI-0653452, and NASA's Outer Planets and Planetary Atmospheres Research programs. We are grateful to R. Laher for use of the RKR code. We thank M. Tashiro for providing tabulations of the DCS calculations of Ref. [5].

[1] Y. Itikawa, J. Phys. Chem. Ref. Data **35**, 31 (2006).
[2] Y. Itikawa, M. Hayashi, A. Ichimura, K. Onda, K. Sakimoto, K. Takayanagi, M. Nakamura, H. Nishimura, and T. Takayanagi, J. Phys. Chem. Ref. Data **15**, 985 (1986).
[3] M. Sataka and H. Kubo, Fusion Sci. Technol. **51**, 135 (2007).
[4] T. Tabata, T. Shirai, M. Sataka, and H. Kubo, At. Data Nucl. Data Tables **92**, 375 (2006).
[5] M. Tashiro and K. Morokuma, Phys. Rev. A **75**, 012720 (2007).
[6] M. A. Khakoo, P. V. Johnson, I. Ozkay, P. Yan, S. Trajmar, and I. Kanik, Phys. Rev. A **71**, 062703 (2005).
[7] P. V. Johnson, C. P. Malone, I. Kanik, K. Tran, and M. A. Khakoo, J. Geophys. Res. **110**, A11311 (2005).
[8] M. A. Khakoo, C. P. Malone, P. V. Johnson, B. R. Lewis, R. Laher, S. Wang, V. Swaminathan, D. Nuyujukian, and I. Kanik, Phys. Rev. A **77**, 012704 (2008).
[9] M. A. Khakoo, S. Wang, R. Laher, P. V. Johnson, C. P. Malone, and I. Kanik, J. Phys. B **40**, F167 (2007).
[10] C. P. Malone, P. V. Johnson, I. Kanik, B. Ajdari, and M. A. Khakoo, J. Chem. Phys. (to be published).
[11] B. R. Lewis, S. T. Gibson, W. Zhang, H. Lefebvre-Brion, and J. M. Robbe, J. Chem. Phys. **122**, 144302 (2005).
[12] M. J. Brunger and P. J. O. Teubner, Phys. Rev. A **41**, 1413 (1990).
[13] D. C. Cartwright, A. Chutjian, S. Trajmar, and W. Williams, Phys. Rev. A **16**, 1013 (1977).
[14] S. Trajmar, D. F. Register, and A. Chutjian, Phys. Rep. **97**, 219 (1983).
[15] M. Zubek and G. C. King, J. Phys. B **27**, 2613 (1994).
[16] C. P. Malone, P. V. Johnson, I. Kanik, B. Ajdari, S. S. Rahman, S. S. Bata, A. Emigh, and M. A. Khakoo, following paper, Phys. Rev. A **79**, 032705 (2009).
[17] M. A. Khakoo, K. Keane, C. Campbell, N. Guzman, and K. Hazlett, J. Phys. B **40**, 3601 (2007).
[18] J. Muse, H. Silva, M. C. A. Lopes, and M. A. Khakoo, J. Phys. B **41**, 095203 (2008).
[19] M. Hughes, K. E. James, J. G. Childers, and M. A. Khakoo, Meas. Sci. Technol. **14**, 841 (2003).
[20] L. R. LeClair and S. Trajmar, J. Phys. B **29**, 5543 (1996).
[21] R. K. Nesbet, Phys. Rev. A **20**, 58 (1979).
[22] E. Schow, K. Hazlett, J. G. Childers, C. Medina, G. Vitug, I. Bray, D. V. Fursa, and M. A. Khakoo, Phys. Rev. A **72**, 062717 (2005).
[23] J. C. Nickel, P. W. Zetner, G. Shen, and S. Trajmar, J. Phys. E **22**, 730 (1989).
[24] A. Lofthus and P. H. Krupenie, J. Phys. Chem. Ref. Data **6**, 113 (1977).
[25] F. R. Gilmore, R. R. Laher, and P. J. Espy, J. Phys. Chem. Ref. Data **21**, 1005 (1992).
[26] R. Laher (private communication).
[27] S. K. Srivastava, A. Chutjian, and S. Trajmar, J. Chem. Phys. **64**, 1340 (1976).
[28] T. W. Shyn and G. R. Carignan, Phys. Rev. A **22**, 923 (1980).
[29] J. C. Nickel, C. Mott, I. Kanik, and D. C. McCollum, J. Phys. B **21**, 1867 (1988).
[30] M. Gote and H. Ehrhardt, J. Phys. B **28**, 3957 (1995).
[31] M. J. Brunger and S. J. Buckman, Phys. Rep. **357**, 215 (2002).
[32] D. C. Cartwright, S. Trajmar, A. Chutjian, and W. Williams, Phys. Rev. A **16**, 1041 (1977).
[33] G. Poparic, M. Vicic, and D. S. Belic, Chem. Phys. **240**, 283 (1999).
[34] J. Mazeau, R. I. Hall, G. Joyez, M. Landau, and J. Reinhard, J. Phys. B **6**, 873 (1973).
[35] L. R. LeClair, S. Trajmar, M. A. Khakoo, and J. C. Nickel, Rev. Sci. Instrum. **67**, 1753 (1996).
[36] A. W. Fliflet, V. McKoy, and T. N. Rescigno, J. Phys. B **12**, 3281 (1979).
[37] G. B. Poparić, M. D. Vićić, and D. S. Belić, Phys. Rev. A **66**, 022711 (2002).
[38] G. Poparić, M. Vićić, and D. S. Belić, Phys. Rev. A **60**, 4542 (1999).